SIMULATION OF MICROSTRUCTURE EVOLUTION DURING WAM PROCESS

J. KRONSTEINER*, H. DREXLER*, S. HOVDEN*, F. HAUNREITER*, P. O'TOOLE**, A. MOLOTNIKOV**, M. EASTON**

**LKR Light Metals Technologies, Austrian Institute of Technology, Giefinggasse 2, 1210 Vienna, Austria*
***RMIT Centre for Additive Manufacturing, School of Engineering, Royal Melbourne Institute of Technology, Melbourne, VIC 3001, Australia*

DOI 10.3217/978-3-85125-968-1-03

ABSTRACT

The development of microstructure during Wire-Based Additive Manufacturing (WAM) is of major interest for the Additive Manufacturing (AM) industry. The resulting geometry, mechanical properties, and quality of WAM parts are directly affected by the process conditions. Numerical simulations of WAM processes can predict and optimize the process settings (heat input, thermal conditions, e.g., by pre-heating, …) and therefore speed-up the trial-and-error phase of the manufacturing process (first time right). The WAM process can be considered as a welding process accompanied by continuous heat-treatment processes (during the build-up of walls the heat source is reheating and even partially remelting existing layers multiple times), the formation of the microstructure mainly depends on the temperature evolution in the part. Two modes of microstructure development are considered: grain nucleation and growth during solidification and growth/recrystallization in the solid phase. To compute grain size considering the interplay of nucleation and growth during solidification, the Interdependence (ID) model is used. Based on the initial grain size distribution, chemical composition, inoculant particles, among other influence factors, the evolution of the microstructure and hot cracking susceptibility during the cooling and reheating cycles of an AM process can be calculated. Both models have been implemented into the Finite Element (FE) solver LS-DYNA®. Depending on the current element temperature either of the two grain morphology models are activated. Here, the evolution of the microstructure including the hot cracking susceptibility during the manufacturing of wall structures is presented. The results obtained from the calculations are compared and validated against our experimental trials. A good agreement between the measured and calculated grain size could be obtained.

Keywords: welding, WAM, microstructure, grain size, solidification

INTRODUCTION

Additive manufacturing (AM) development activities have increased dramatically during the last few years. There are several reasons for this major interest from industry and academia. Especially in sectors such as aerospace, medical and tooling industries, the following advantages are of interest [1]:

- AM processes have in general superior mechanical properties in comparison to cast counterparts,

- AM enables manufacturing of complex 3D geometries often obtained by topology optimization and integrating structures with recesses and additional functionalities such as cooling channels,
- potential reduction in weight due to optimized material usage and/or expensive light metals such as high-performance aluminum or titanium alloys and therefore reduced CO_2 emissions,
- near net shape manufacturing (depending on the process),
- reduction in scrap material compared to forming and/or machining processes,
- improved properties due to extreme solidification conditions resulting in unique microstructure [2],
- engineering of microstructure during AM processing [2],
- and many more.

Due to the different requirements for different fields of applications, there is a multitude of additive manufacturing methods on the market today. Powder based additive manufacturing methods for metals can maintain very strict geometrical tolerances and therefore high surface quality requirements. However, part size is usually restricted by the AM machine. Most laser-based systems additionally have a maximum build rate in the range of 70-100 cm^3/h and a limited build volume in the range of 40 x 40 x 40 cm^3 [1,3]. Metal deposition techniques such as laser metal deposition (LMD) and the wire additive manufacturing (WAM) only have very little restrictions on the build size and have the highest build rates of all AM techniques [1]. It is also possible to use graded and hybrid materials by feeding different filler materials simultaneously. However, in terms of geometrical tolerances and surface roughness, these methods are inferior to most powder-based methods. The surface roughness ranges between 10 Ra and 200 Ra but the build rates can be up to 300 cm^3/h [1].

Whenever large components and a high throughput are favored, WAM is a good choice. This is one of the reasons why WAM is used in this publication. Since wire-based AM processes are in principle welding processes (either using laser, plasma or as in the presented case electric arc) they are thus susceptible to certain defects. Metals which can be processed by WAM need to have good weldability to avoid cracks during solidification.

In addition to titanium and steel, an increasing research activity is visible regarding high-performance aluminum alloys for WAM applications. Due to the key role of 6xxx series alloys for the automobile industry, the implementation of compatible WAM feedstock wire is of major interest [5]. Especially Al-Mg-Si alloys of the 6xxx series, however, show a tendency for hot cracking [4-6]. Hot Cracking is caused by the predominant tensile stresses in the mushy zone due to shrinkage and its interaction with liquid feeding [7]. Liquid feeding has been visualized for steel by Agrawal et al. [8] using in-situ microscopic methods. Since hot cracks originate in the final state of solidification in the semisolid region due to localized applied load, the modelling of the mechanical behavior is of utmost importance [9]. The localized load or even strain or strain rate can occur due to constrained thermal contraction and the density change from liquid to solid [9]. Liquid feeding can compensate for the shrinkage during cooling at low solid fractions. The higher the solid fractions, the more difficult the interdendritic feeding becomes and the higher the chance for hot cracks to occur [9]. Voids can then nucleate

and grow into cracks under a certain applied load [9]. There is also a considerable influence of the alloy composition, especially for aluminum alloys. The interaction between nucleants and solutes was investigated by Easton and StJohn [10, 11]. The Interdependence Theory links grain formation and nucleation selection [12, 13].

In addition to the solidification conditions, WAM processed materials are characterized by the process-intrinsic heat treatment [14]. These heat treatment processes affect solid-state precipitation reactions and thus mechanical properties [15]. In aluminum alloys, this thermal treatment additionally results in grain coarsening reactions [15]. The main focus of this paper is therefore to model the grain coarsening behavior during AM processing on a part-scale using Finite Element (FE) methods.

MATERIAL MODELLING

To ultimately model the grain size distribution and the susceptibility for hot cracking effects after WAM processing, several numerical methods need to work together. In this work grain formation is calculated by the Interdepence Theory (ID, [12]) while solid-state grain growth is considered using a static recrystallization (ReX) and grain morphology model [16]. The mechanical behavior in the solid state is covered by a dislocation density-based flow stress model [16]. The hot cracking susceptibility is calculated based on the critical strain rate and given by a dimensionless indicator based on the minimal (in plane) strain rate.

Finally, the welding process is covered by a special heat source and element activation technique.

INTERDEPENDENCE THEORY (ID)

The ID model [12] considers the formation and growth of new grains as depending on the chemical composition of the alloy, the average distance, number and efficiency of activated inoculant particles, the effect of constitutional supercooling regeneration, critical nucleation undercooling on varying inoculant diameters, interface growth velocity and growth restriction factor, among others. The ID links together the nucleation and growth during the initial transient, demonstrating that the nucleation, growth, and activation or inhibition of neighboring heterogenous substrates depends on the growth restriction factor and the growth required to establish constitutional supercooling, x_{CS}, the diffusion length, x_{l_D}, and the average distance between potent inoculant particles, x_n, [12]. For a given inoculated alloy, the grain size can be computed as the sum of these components, by

$$d_g = x_{CS} + x_{l_D} + x_n, \tag{1}$$

These lengths depend on material and process parameters and, as such, link the material response to the process conditions. The terms x_{CS}, x_{l_D}, and x_n are computed by the following equations,

$$x_{CS} = \frac{D_l z \Delta T_n}{vQ}, \tag{2}$$

$$x_{l_D} = \frac{4.6 D_l}{v}\left(\frac{c_L - c_0}{c_L(1-k)}\right), \tag{3}$$

$$x_n = \frac{1}{\sqrt[3]{f N_v}}. \tag{4}$$

where D_l is the liquid diffusion constant, ΔT_n is the nucleation temperature computed by Greer's Free Growth model [17], v is the solidification velocity, Q is the growth restriction factor [18], c_0 and c_L are the nominal alloy composition and the maximum liquid composition at the interface, k is the partition coefficient, N_v is the volume density of inoculant particles in m^{-3}, and f is the relative efficiency of the inoculant. This model has seen broad application to explain nucleation and growth of grains in several alloy systems, including aluminum alloys. To compute the morphology of grains, the grain size is compared to the secondary dendrite arm spacing, λ_2, computed by,

$$\lambda_2 = 5.5[M \cdot t_f]^{-n}, \tag{5}$$

where t_f is the freezing time, obtained from the process model and assumptions about the mush (see the hot cracking section below), n is a known material constant between 0.3 and 0.5, and M is computed from the Gibbs-Thomson coefficient and the value of the growth restriction factors at $f_s \sim 0$ and $f_s \sim f_{eutectic}$, respectively $Q_{0,j}$ and $Q_{f,j}$, by [19],

$$M = \frac{\Gamma}{\sum_{j=1}^{n}(Q_{0,j} - Q_{f,j})/D_j} ln\left[\frac{\sum_{j=1}^{n} -Q_{f,j}/D_j}{\sum_{j=1}^{n} -Q_{0,j}/D_j}\right] \tag{6}$$

HOT CRACKING MODEL

A modified Rappaz-Drezet-Gremaud hot tearing model is used [20] to compute the critical strain rate which is compared to the calculated strain rate in the FE simulation. This model computes the critical strain rate for an alloy solidifying with an equiaxed morphology by considering the ability of the viscous liquid above a growing field of grains to feed the diminishing mush, sufficient to offset solidification shrinkage. This critical strain rate, $\dot{\varepsilon}_{critical}$, is computed by,

$$\dot{\varepsilon}_{critical} = \frac{{d_g}^2}{180(1+\beta)B\mu L^2}\left(p_m - \frac{4\gamma}{\lambda_2\left(1-\sqrt[3]{f_{ca}}\right)}\right) - \frac{v\beta A}{(1+\beta)BL} \tag{7}$$

where β is the solidification shrinkage, μ is the viscosity, p_m is the metallostatic pressure, γ is the liquid-void surface tension, d_g is the secondary dendrite arm spacing (or the equiaxed grain size), v is the solid front isotherm velocity and L is the length of the mushy zone. The term f_{ca} is the solid fraction where adjacent grains coalesce at the final moments of solidification. The terms, F, A, and B, are computed over the mush length from the temperature at the *coherence* solid fraction, $T_{co}(f_{co})$, where strain can be communicated across the mush and the temperature at *coalescence* $T_{ca}(f_{ca})$, by

$$A = \Delta T^{-1} \int_{T_{ca}}^{T_{co}} \frac{f_s(T)^2}{\left(1-f_s(T)\right)^2} dT \tag{8}$$

$$B = \Delta T^{-1} \int_{T_{ca}}^{T_{co}} \frac{\left(1-f_s(T)\right)^2 F(T)}{\left(1-f_s(T)\right)^3} dT \tag{9}$$

$$F = \Delta T^{-1} \int_{T_{ca}}^{T_{co}} f_s(T)\, dT \tag{10}$$

$$\Delta T = T_{co} - T_{ca}. \tag{11}$$

The solid fraction versus temperature curves, $f_s(T)$, are computed by Scheil calculation of solidification obtained from JMatPro (Sente Software, UK) [21]. All basic thermophysical properties are obtained from this calculation.

FLOW STRESS MODEL

As already mentioned in the introduction, hot cracking, but also solid-state grain growth, needs a certain localized load to be promoted. To model the response to mechanical loading, a flow stress model was implemented in the context of FE methods. The so-called mean dislocation density material (MD²M) model is based on capturing the localized evolution of mean dislocation density depending on strain, strain rate and temperature. In the case of Additive Manufacturing (AM), the loading originates from the restricted thermal contraction due to the mechanical clamping of the substrate in AM processes. This is also one of the main sources for residual stresses which subsequently influence the hot cracking susceptibility.

The constitutive stress-strain model is commonly written as a sum of an initial yield (threshold) stress, σ_y, and a strain-dependent part, σ_ρ. The latter might be described in a power law form or by using an internal state parameter-based model. In present work we will follow a Kocks-Mecking approach [22,23], which is based on an evolution of the dislocation density ρ:

$$\sigma = \sigma_y + M \cdot b \cdot G \left(\alpha\sqrt{\rho} + \frac{1}{\delta}\right) \tag{1}$$

The second part in Eq. (1) represents the strain dependent part (σ_ρ). During deformation, the material substructure with a mean sub-grain size (δ) is formed influencing the third part of Eq. (1) and is inversely proportional to $\sqrt{\rho}$. Variables and parameters in Eq. (1) and the following equations are summarized in Table 1. The change in the mean dislocation density by deformation at temperature, T, with a strain rate, $\dot{\varphi}$, might be described as a superposition of dislocations production and their annihilation [24-27] as following:

$$\frac{\mathrm{d}\rho}{\mathrm{dt}} = \frac{\mathrm{M}\sqrt{\rho}}{\mathrm{b}\cdot\mathrm{A}}\dot{\varphi} - 2\mathrm{B}\frac{\mathrm{d_{ann}}}{\mathrm{b}}\rho\mathrm{M}\dot{\varphi} - 2\mathrm{CD}\frac{\mathrm{Gb}^3}{\mathrm{k_B T}}\left(\rho^2 - \rho_{\mathrm{eq}}^2\right) \tag{2}$$

While the first term corresponds to the increase in dislocation density, the last two terms describe the recovery process by spontaneous annihilation and thermally activated dislocation climb.

The first recovery process happens when two dislocations with antiparallel Burgers vectors come to a critical distance, d_{ann}, while the second one is thermally activated and controlled by self-diffusion along the dislocations, D.

Furthermore, equation (2) contains three calibration parameters (A, B, C). A is a material constant depending on the purity, B is associated with the number of activated slip planes and C considers the solute trapping [24]. For simplicity, however, these parameters are normally tuned using the experimental stress–strain curves.

GRAIN MORPHOLOGY MODEL

The calculation of the developing microstructure is mainly based on the simulation of grain/subgrain growth and is implemented in the second part of the MD²M model. Here, a distinction is made between the grain growth of already existing grains δ^{G} from the melt and recrystallized grains δ^{rex}. The growth of existing grains is described by the following expression:

$$\frac{\mathrm{d}\delta^{\mathrm{G}}}{\mathrm{dt}} = 2 \cdot \mathrm{M}_{\mathrm{GB}} \cdot \left(\frac{3 \cdot \gamma}{\delta^{G}} + P_D - P_Z\right) \tag{3}$$

In a similar manner, the recrystallized grains δ^{rex} can grow according to:

$$\frac{\mathrm{d}\delta^{\mathrm{rex}}}{\mathrm{dt}} = 2 \cdot \mathrm{M}_{\mathrm{GB}} \cdot (P_D - P_Z) \cdot (1 - X), \tag{4}$$

and the subgrain size δ^{S} evolves due to:

$$\frac{\mathrm{d}\delta^{S}}{\mathrm{dt}} = 2 \cdot \mathrm{M}_{sub} \cdot (P_D - P_Z) \cdot (1 - X). \tag{5}$$

Table 1 MD²M model variables and physical constants used in Eqs. (1-5).

Description	Variable name	Values	Units
Taylor factor for fcc textures	M	3.06	[-]
Length of the Burgers vector	b	28.6	[nm]
Boltzmann constant	k_b	1.381E-23	[J K^{-1}]
Diffusion coefficient in solid state	D_s	calculated	[m^2 s^{-1}]
Temperature dependent shear modulus	G(T)	calculated	[Pa]
Grain size	$(\delta_0^G), \delta^G$	calculated	[m]
(Initial) grain size (e. g. from casting)	d_g	calculated	[m]
Flow stress (y… yield)	σ, σ_y	calculated	[Pa]
Dislocation density (eq…equilibrium)	ρ, ρ_{eq}	calculated	[m^{-2}]
Accumulated dislocation density	ρ_g	calculated	[m^{-2}]
Stored energy (in microstructure)	P_D	calculated	[Pa]
Mobility of grain and subgrain boundaries	M_{GB}, M_{sub}	calculated	[m^2 s kg^{-1}]
Zener pressure (in grains, subgrains)	P_Z,$P_{Z,sub}$ [16,17]	calculated	[Pa]
Recrystallized fraction	X	calculated	[-]
Critical distance for spontaneous annihilation	d_{ann}	calculated	[m]
Subgrain size (eq…equilibrium)	δ^S, δ_{eq}^S	calculated	[m]
Grain/Subgrain boundary energy	γ, γ^S	calculated	[J m^{-2}]
Alloy specific parameters	α, A, B, C, K	calculated	[-]
Plastic strain	φ	calculated	[-]
Local strain rate	$\dot{\varphi}$	calculated	[s^{-1}]
Temperature	T	calculated	[K]
Time, time step	t, dt	calculated	[s]

NUMERICAL WELDING MODEL

When all the models are run together in one framework, welding processes of considerable part sizes can be investigated in detail. Firstly, the elements of the current layer were inserted by the SAM (Simulation of Additive Manufacturing, [28]) framework in a quiet state. The welding process was then simulated by the LS-DYNA® solver using a Goldak [29] heat source. When the heat source passed over the quiet elements, element activation occurred depending on the element temperature. Similar to the *MAT_CWM [30] implementation (CWM ds for Computational Welding Mechanics) in LS-DYNA®, a user-defined variant was implemented for the mechanical case. Between start (S_{mech}) and end temperature (E_{mech}), mechanical properties such as Young's modulus, Poisson ratio, yield stress and thermal expansion coefficient were linearly scaled from "ghost" to realistic values (see Fig. 1 (a)). The main reason for writing a user-defined variant of *MAT_CWM was to combine all the above models together (see Fig. 2), which is only possible by applying a user-defined material model. For the activation of the thermal material properties, conventional *MAT_THERMAL_CWM, implemented in LS-DYNA®, was used.

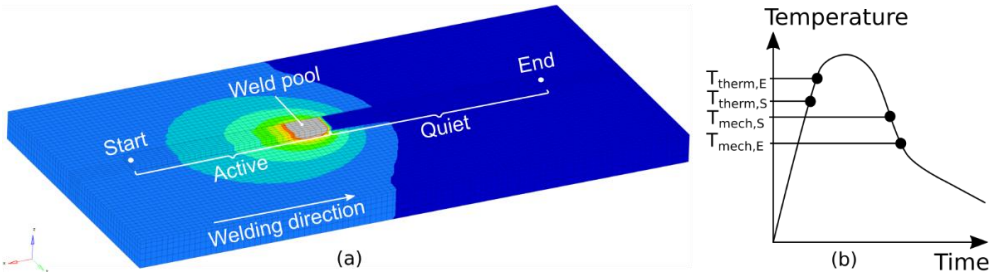

Fig. 1 Application of the quiet element method for temperature results (a) and diagram showing the thermal and mechanical activation procedure (b)

Here again, thermal properties such as specific heat, thermal conductivity, among others, were linearly scaled between "ghost" and realistic values. Temperature dependent curves were used for the thermal and mechanical properties which were not calculated.

During the mechanical element activation process (between $T_{mech,S}$ and $T_{mech,E}$), interdependence and hot cracking models were activated. To correctly consider the contraction of the cooling material after solidification in combination with the MD²M model, the activation procedure for the user-defined mechanical CWM model was modified.

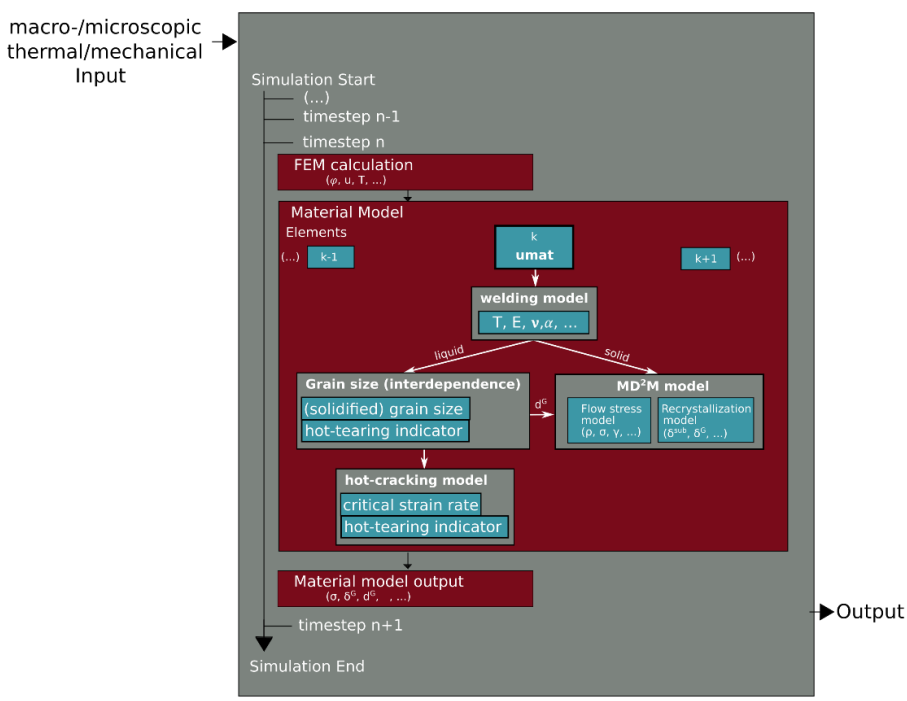

Fig. 2 Diagram showing the implemented models and the most important variables/parameters

Since the expansion of the material during heating could lead to generation of dislocations even during the "melting" of the material drop, $T_{mech,S}$ and $T_{mech,E}$ were defined in such a way that element activation could only happen during the cooling of the molten material (see Fig. 1 (b)) in the mechanical case. The activation of the thermal material properties happened during heating (which is the standard implementation in LS-DYNA®) between $T_{therm,S}$ and $T_{therm,E}$. The contraction of the solidified material led to plastic deformation and thus the production of dislocations due to residual stresses.

Based on the chemical composition, inoculant particles, among other influence factors, the initial microstructure was calculated by the interdependence model during the cooling of the molten material. In areas where the material was already solidified, the grain morphology was further described by the grain growth model which was adapted for AM applications by LKR. When the welding process (including a certain holding time between layers) was finished, the LS-DYNA® simulation was finished too and a new layer (already pre-meshed) was inserted by the SAM framework. After finishing the preparations for the new run, the SAM framework restarted the thermo-mechanical simulation again. This process was repeated until the pre-defined number of layers (48) were produced. The relationship between the models and how they are connected is illustrated in Fig. 2.

SIMULATION MODEL SETUP

The setup for the simulation model of a simple wall structure was designed in a way to closely resemble the real setup in the workshop (see Fig. 3).

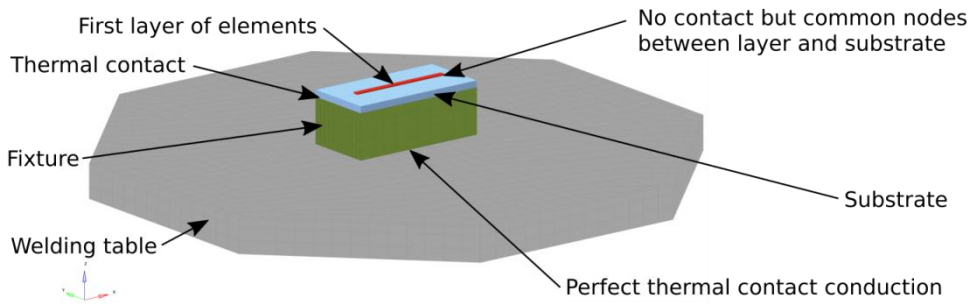

Fig. 3 Model setup for the WAM simulation of a single wall

Due to the importance of the thermal conditions during WAM processing, the fixture and the welding table were considered as well. In that way, the heat flux into the fixture and the welding table could be taken care of. A combination of convection and radiation was used to set the boundary conditions for the model. Due to the large range of temperatures, the values for convection and radiation were combined into a temperature dependent curve for the convection boundary condition including the effect of radiation [31,32]. This combined approach allows to use °C in the model whereas LS-DYNA® asks

for K when using radiation. The user-defined material models internally convert °C from the model in K.

The heat transfer coefficient (HTC) for the thermal contact between the different parts/materials is hard to define since it depends on temperature, pressure and surface roughness. The HTCs used in this model are based on a correlation of temperature from experiments performed with the same setup and numerical simulations thereof. An HTC of 1000 $Wm^{-2}K^{-1}$ was used for the thermal contact between substrate and fixture, whereas perfect thermal contact conduction was defined between the fixture and the welding table. To achieve a suitable interlayer temperature, two preheating runs were performed by moving the heat source over the substrate without adding material. This is a procedure which is also performed in the experiments and helps to reduce the heat loss into the whole setup.

A mechanical surface to surface contact was used between substrate, fixture, and welding table. The connection between the individual layers was implemented by using common nodes between the elements of the existing and the new layer.

RESULTS AND DISCUSSION

In the following section we will discuss first the experimental and afterwards the simulation results. The experiments were performed by the project partner RHP-Technology GmbH. The simulation work was performed by LKR using a Linux-based cluster and the commercial LS-DYNA® FEM solver with implemented user-defined material models as described in the section Material Modelling. The build-up process was simulated for 48 layers up to a height of 91.5 mm.

EXPERIMENTAL RESULTS

By using a plasma metal deposition (PMD) process, RHP produced a wall by welding several layers atop another until a wall was generated (see Fig. 4).

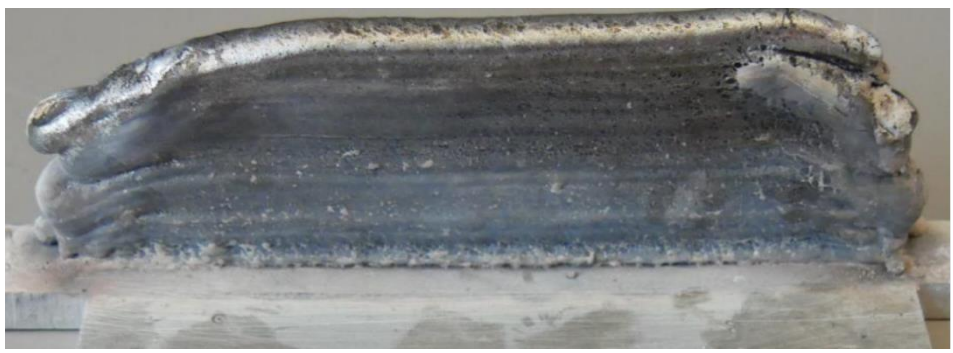

Fig. 4 Wall samples made from nano-treated 6061NT material

Micrographs of two positions of a section through this wall are given in Fig. 5. A very homogeneous distribution of very fine grains could be found as shown in Fig. 5 (a) and (b).

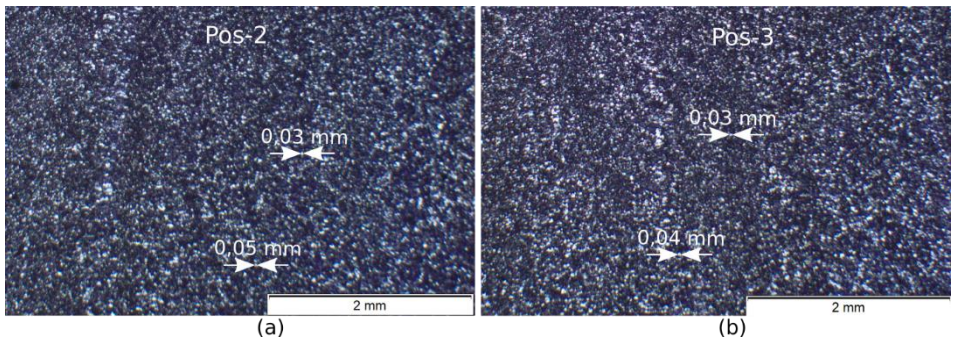

Fig. 5 Optical Micrographs of pos-2 (a) and pos-3 (b) from Barker etched 6061NT wall samples

The final grain sizes which could be found from the micrographs are in the area of 0.01 to 0.1 mm diameter.

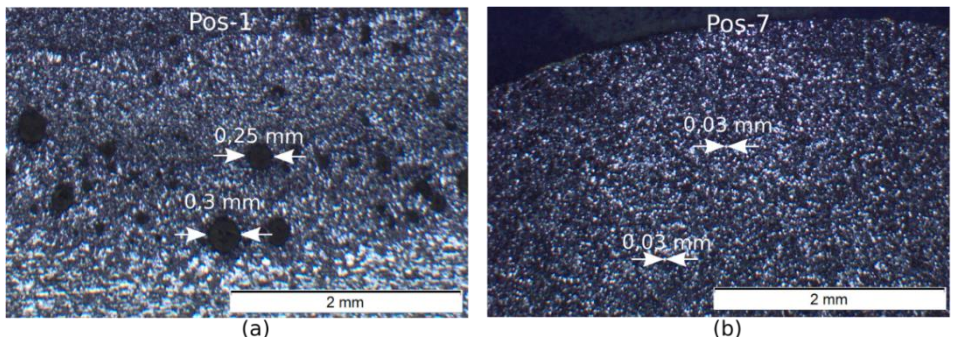

Fig. 6 Optical Micrograph of bottom (a) and top (b) in Barker etched 6061NT wall samples

Minor voids at the bottom near the interface between substrate and wall are visible in Fig. 6 (a). At the top of the wall (Fig. 6 (b)), the microstructure is still void-free and shows grains of approximately 0.03 mm.

NUMERICAL RESULTS

Similar to the experimental procedure, the simulation started with two pre-heating runs. Using only the torch (or the Goldak heat source in the simulation), substrate, fixture and welding table were preheated to reduce the heat loss for the first layer and to help get good bonding between the welding material and the substrate (see Fig. 7).

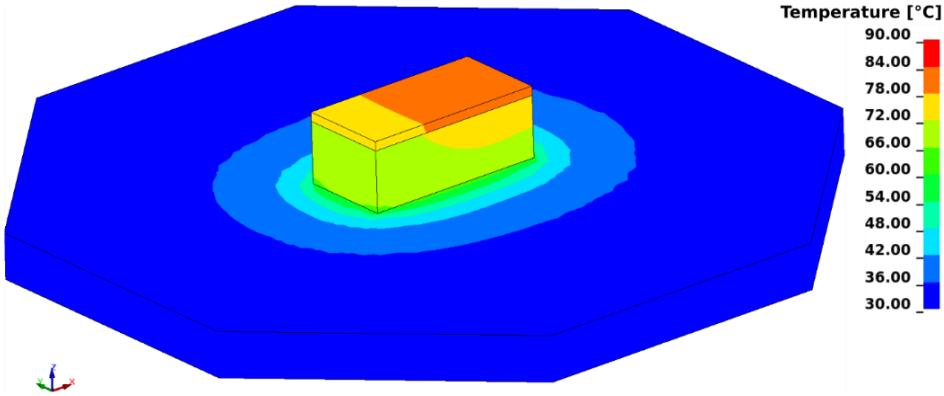

Fig. 7 Initial temperature distribution of the whole setup after pre-heating

The already pre-activated elements of the substrate were heated during pre-heating to reduce the heat loss during welding. When the first layer was connected to the substrate, the heat loss due to the shared nodes between first layer elements and substrate elements was thus reduced by the pre-heating.

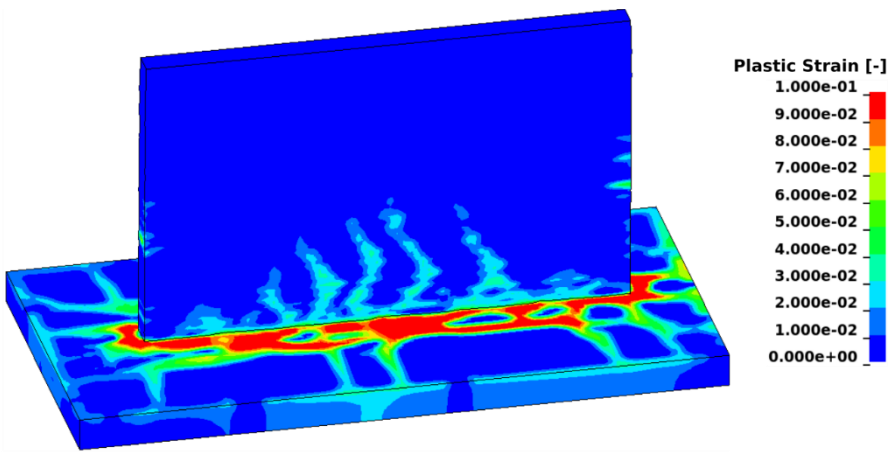

Fig. 8 Plastic strain distribution after welding of 48 layers including time for cooling

The plastic strain distribution due to the contracting material during cooling is given in Fig. 8 and shows plastic strains near the bottom part of the wall.

The resulting dislocation density distribution due to the plastic strain and temperature is given in Fig. 9. The A, B and C parameters for modelling the stress-strain behavior for the specific alloy was found by curve fitting using the flow curves of 6061NT for several strain rates and temperatures.

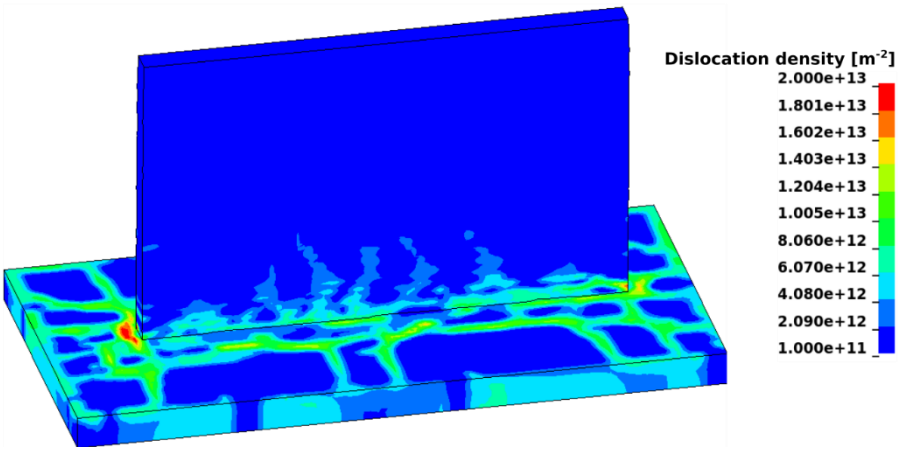

Fig. 9 Distribution of dislocation density after welding of 48 layers including time for cooling

When the temperature during cooling falls below a critical temperature, the Interdependence model starts calculating the initial grain size coming from the melt. The distribution of initial grain size for 48 layers is illustrated in Fig. 10.

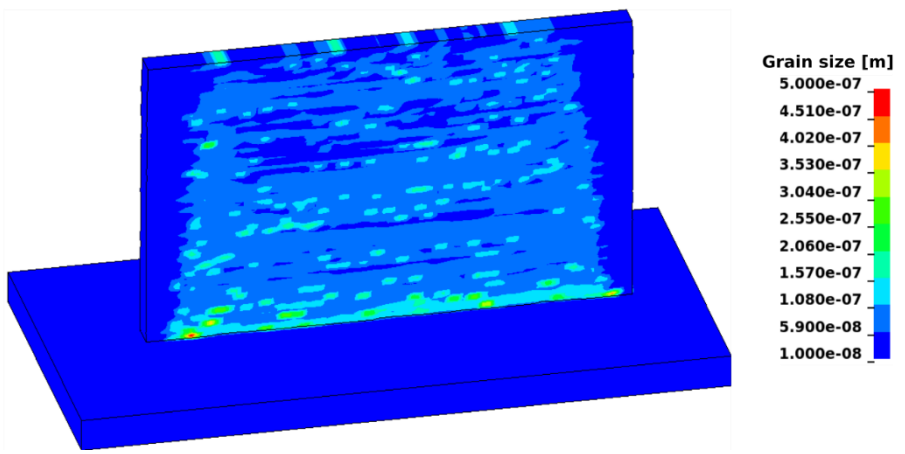

Fig. 10 Grain size distribution from the interdependence model after welding of 48 layers

When the material is fully solidified, the grain morphology model calculates the grain size evolution during cooling and re-heating. The resulting grain size distribution after welding of 48 layers can be found in Fig. 11. There is a good agreement for the final grain size between experiments and simulations.

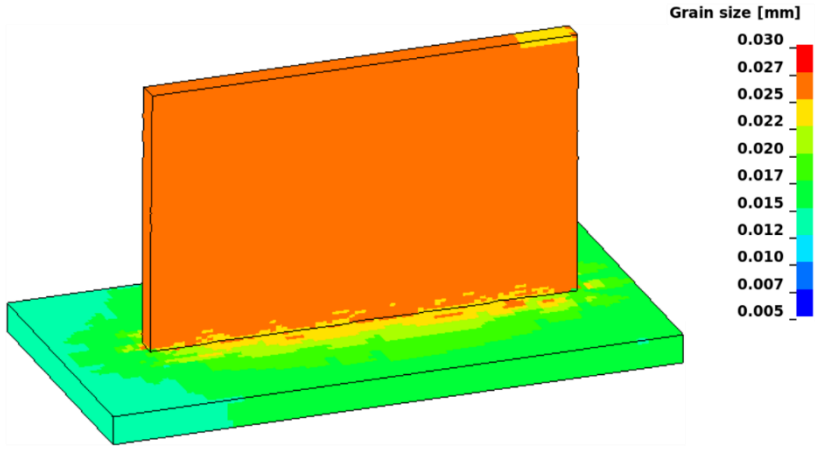

Fig. 11 Grain size distribution from the grain morphology model after welding of 48 layers

The resulting distribution of residual stresses shows higher values near the wall edges and in general at the bottom and in the base plate (see Fig. 12).

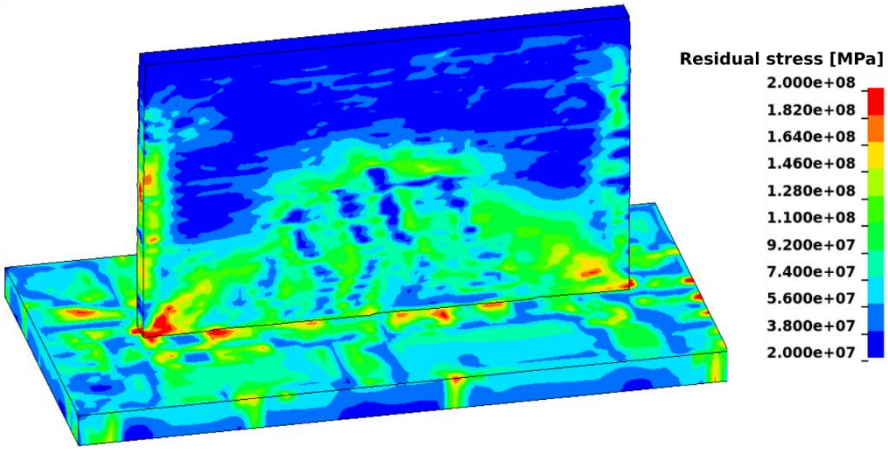

Fig. 12 Distribution of residual stress in the substrate with the first 48 layers

Finally, the hot cracking model continuously calculates the hot cracking susceptibility. As can be seen in Fig. 13, the probability for hot cracking is especially high near the edges of the walls. With increasing wall height, the critical strain rate grows from the edges in the direction of the center of the wall.

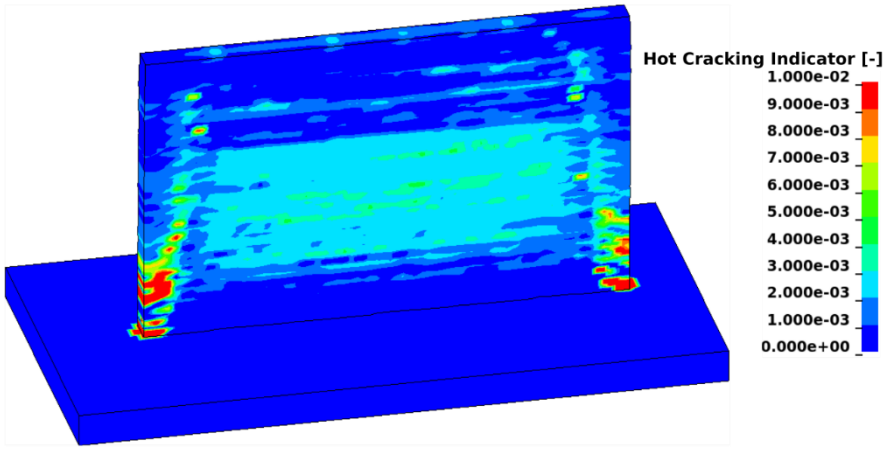

Fig. 13 Hot Cracking susceptibility for a wall of 91.5 mm height

CONCLUSION

In the here presented first results from the thermo-mechanical WAM process model, several models could be successfully implemented and coupled to calculate the macro- and microstructure results from the molten material until the failure of the part due to distortion, residual stress and the hot cracking susceptibility. Although further testing and calibration are necessary, reasonable results could already be obtained. Proper validation is also still pending and the application to different geometries and alloys is also a major question. Further tasks are a mesh and timestep sensitivity study in order to reduce the calculation times. With implicit timesteps of 0.25 s for the welding simulation, the fully coupled model takes approximately one 3 hour 15 minutes for a representative layer using 4 nodes on a Linux cluster with 16 cores each.

APPENDICES AND ACKNOWLEDGEMENTS

The authors would like to thank Austrian Research Promotion Agency (FFG) for sponsoring the research work in the project M4AM (funding scheme: Beyond Europe: 874169), Austrian Federal Ministry for Climate Action, Environment, Energy, Mobility, Innovation and Technology and the Austrian Institute of Technology (AIT) for the technical/financial support in this research work. Special thanks to RHP-Technology GmbH for performing the experimental work during the M4AM project.

References

[1] S. GORSSE, C. HUTCHINSON, M. GOUNÉ AND R. BANERJEE: 'Additive manufacturing of metals: a brief review of the characteristic microstructures and properties of steels', Ti-6Al-4V and high-entropy alloys, *Science and Technology of Advanced Materials*, Vol.18, No. 1, pp. 584-610, 2017.

[2] A. PRASAD, L. YUAN, P. LEE, M. PATEL, D. QIU, M. EASTON, D. ST JOHN: 'Towards understanding grain nucleation under additive manufacturing conditions', *Acta Materialia*, Vol. 195, pp. 392-403, 2022.

[3] A. M. KHORASANI, I. GIBSON, J. K. VEETIL, A. H. GHASEMI: 'A review of technological improvements in laser-based powder bed fusion of metal printers', *International journal of advanced manufacturing technology*, Vol. 108, No. 1-2, pp. 191-209, 2020, https://doi.org/10.1007/s00170-020-05361-3.

[4] L. SWEET, M. A. EASTON, J. A. TAYLOR, J. F. GRANDFIELD, C. J. DAVIDSON, L. LU, M. J. COUPER AND D. H. STJOHN: 'Hot Tear Susceptibility of Al-Mg-Si-Fe Alloys with Varying Iron Contents', *TMA and ASM International*, 2012, https://doi.org/10.1007/s11661-012-1562-1.

[5] T. KLEIN, A. ARNOLDT, R. LAHNSTEINER, M. SCHNALL: 'Microstructure and mechanical properties of a structurally refined Al–Mg–Si alloy for wire-arc additive manufacturing', *Materials Science & Engineering A*, Vol. 830, 142318, 2022.

[6] C. HAGENLOCHER, D. WELLER, R. WEBER, T. GRAF: 'Reduction of the hot cracking susceptibility of laser beam welds in AlMgSi alloys by increasing the number of grain boundaries', *Science and Technology of Welding and Joining*, Vol. 24, No. 4, pp. 313-319, 2019.

[7] N. CONIGLIO, C. E. CROSS: 'Mechanisms for solidification crack initiation and growth in aluminum welding', *Int. Mater. Rev.*, Vol. 58, pp. 375-397, 2013, https://doi.org/10.1179/1743280413Y.0000000020.

[8] G. AGARWAL, M. AMIRTHALINGAM, S.C. MOON, R. J. DIPPENAAR, I. M. RICHARDSON, M. J. M. HERMANS: 'Experimental evidence of liquid feeding during solidification of a steel', *Scripta Mater.*, Vol. 146, pp. 105-109, 2018, https://doi.org/10.1016/j. scriptamat.2017.11.003.

[9] M. A. EASTON, ET AL.: 'Observation and Prediction of the Hot Tear Susceptibility of Ternary Al-Si-Mg Alloys', *The Minerals, Metals & Materials Society and ASM International*, 2012, https://doi.org/10.1007/s11661-012-1132-6.

[10] M. A. EASTON, D. H. STJOHN: 'A model of grain refinement incorporating alloy constitution and potency of heterogeneous nucleant particles', *Acta Mater.*, Vol. 49, pp. 1867-1878, 2001, https://doi.org/10.1016/S1359-6454(00)00368-2.

[11] M. A. EASTON, D. H. STJOHN: 'An analysis of the relationship between grain size, solute content, and the potency and number density of nucleant particles', *Metall. Mater. Trans. A Phys. Metall. Mater. Sci.*, Vol. 36, pp. 1911-1920, 2005, https://doi.org/10.1007/s11661-005-0054-y.

[12] D. H. STJOHN, M. QIAN, M. A. EASTON, P. CAO: 'The Interdependence Theory: the relationship between grain formation and nucleant selection', *Acta Mater.*, Vol. 59, pp. 4907-4921, 2011, https://doi.org/10.1016/j.actamat.2011.04.035.

[13] M. BERMINGHAM, D. STJOHN, M. EASTON, L. YUAN, M. DARGUSCH: 'Revealing the mechanisms of grain nucleation and formation during additive manufacturing', *JOM (J. Occup. Med.)*, Vol 72 pp. 1065-1073, 2020, https://doi.org/10.1007/s11837- 020-04019-5.

[14] K. OYAMA, S. DIPLAS, M. M'HAMDI, A.E. GUNNÆS, A.S. AZAR: 'Heat source management in wire-arc additive manufacturing process for Al-Mg and Al-Si alloys', *Addit. Manuf.*, Vol. 26, pp. 180-192, 2019, https://doi.org/10.1016/j.addma.2019.01.007.

[15] T. KLEIN, M. SCHNALL: 'Control of macro-/microstructure and mechanical properties of a wire-arc additive manufactured aluminium alloy', *Int. J. Adv. Manuf. Technol.*, Vol. 108, pp. 235-244, 2020, https://doi.org/10.1007/s00170-020-05396-6.
[16] P. SHERSTNEV, C. MELZER, C. SOMMITSCH: 'Prediction of precipitation kinetics during homogenisation and microstructure evolution during and after hot rolling of AA5083', *Int. J. of Mech. Sci.*, Vol 54, pp. 12-19, 2012, https://doi.org/10.1016/j.ijmecsci.2011.09.001.
[17] A. L. GREER, A. M. BUNN, A. TRONCHE, P. V. EVANS, D. J. BRISTOW: 'Modelling of inoculation of metallic melts: application to grain refinement of aluminium by Al-Ti-B', *Acta Mater.*, Vol. 48, pp. 2823-2835, 2000.
[18] I. MAXWELL, A. HELLAWELL: 'A simple model for grain refinement during solidification', *Acta Metall.*, Vol. 23/2, pp. 229-237, 1975.
[19] M. EASTON, C. DAVIDSON, D. STJOHN: 'Effect of Alloy Composition on the Dendrite Arm Spacing of Multicomponent Aluminum alloys', *Metall. and Mat. Tran. A*, Vol. 41A, pp. 1528-1538, 2010.
[20] M. RAPPAZ, J.-M. DREZET, M. GREMAUD: 'A new hot-tearing criterion', *Metall. and Mat. Trans. A*, Vol. 30/A, pp. 449-455, 1999.
[21] N. SAUNDERS, U. K. Z. GUO, X. LI, A. P. MIODOWNIK, J. -PH. SCHILLÉ: 'Using JMatPro to model materials properties and behavior', *JOM*, Vol. 55, pp. 60-65, 2003, https://doi.org/10.1007/s11837-003-0013-2.
[22] U. F. KOCKS: 'Laws for Work-Hardening and Low-Temperature Creep', *ASME. J. Eng. Mater. Technol.*, Vol. 98(1), pp. 76-85, 1976, https://doi.org/10.1115/1.3443340.
[23] H. MECKING, U. F. KOCKS: 'Kinetics of flow and strain-hardening', *Acta Metallurgica*, Vol. 29, pp. 1865-1875, 1981.
[24] P. SHERSTNEV, P. LANG, E. KOZESCHNIK: 'Treatment of simultaneous deformation and solid-state precipitation in thermo-kinetic calculations', *ECCOMAS Proceedings*, pp. 5331-5338, 2012.
[25] E. KABLIMAN, P. SHERSTNEV: 'Integrated Modeling of Strength Evolution in Al-Mg-Si Alloys during Hot Deformation', *Mat. Sci. For.*, Vol. 765, pp. 429-433, 2013.
[26] E. KABLIMAN, P. SHERSTNEV, J. KRONSTEINER, T. EBNER: 'Physikalisch basierte Simulation des Rekristallisationsverhaltens in einer Al-Cu-Mg-Mn Legierung während der Warmumformung und anschließender Wärmebehandlung', *Tagungsband der 8. Ranshofener Leichtmetalltage*, edited by C. M. Chimani et al., pp. 50-60, 2014.
[27] J. KREYCA, E. KOZESCHNIK: 'State parameter-based constitutive modelling of stress strain curves in Al-Mg solid solution', *Int. J. Plast.*, Vol. 103, pp. 67-80, 2018.
[28] S. BROETZ, A. M. HORR: 'Framework for progressive adaption of FE mesh to simulate generative manufacturing processes', *Manufacturing Letters*, Vol. 24, pp. 52-55, 2020, https://doi.org/10.1016/j.mfglet.2020.03.005.
[29] J. GOLDAK, A. CHAKRAVARTI, M. BIBBY: 'A new finite element model for welding heat sources', *Int. Metal. Trans. B*, Vol. 15, pp. 299-305, 1984.
[30] P.LINDSTRÖM: '*Improved CWM platform for modelling procedures and their effects on structural behavior*', PhD Thesis, Production Technology, University West, 2015.
[31] F. HAUNREITER: '*Numerisch basierte Schweißleistungsvorhersage für den WAM-Prozess*', Master Thesis, University of Applied Sciences FH Technikum Wien, 2021.
[32] Y. CENGEL: 'Introduction to the thermodynamics and heat transfer', *McGraw-Hill Education*, 2008.